

Improved Constraints on the Variation of the Weak Scale from Big Bang Nucleosynthesis

Helen Meyer¹ and Ulf-G. Meißner^{1,2}

¹*Helmholtz-Institut für Strahlen- und Kernphysik and Bethe Center for Theoretical Physics,
Universität Bonn, D-53115 Bonn, Germany*

²*Institute for Advanced Simulation, Forschungszentrum Jülich, D-52425 Jülich, Germany*

(Dated: March 15, 2024)

We analyze the recent EMPRESS data on the ^4He abundance in Big Bang nucleosynthesis as a function of the Higgs vacuum expectation value v and compare our calculation to the recently published work of Burns et al. [1]. The EMPRESS result for the ^4He abundance can be explained within 2σ by $0.03 \leq \delta v/v \leq 0.07$. However, as first noted in [1], a Higgs VEV in this range would worsen the discrepancy between theory and experiment for the deuterium abundance significantly.

I. INTRODUCTION

Big Bang nucleosynthesis (BBN) is a fine laboratory for the possible variations of the fundamental constants of nature, see e.g. [2–7]. In a recent publication [1], Burns et al. studied possible constraints on a variation of the Higgs vacuum expectation value (VEV) from BBN simulations. They use the new PRyMordial code [8] to compute the Helium-4 (^4He) and deuterium (d) abundances for different values of the Higgs VEV and compare their results to the newest observation by the EMPRESS collaboration [9] that differs from the values given by the Particle Data Group (PDG) [10] and from current theoretical predictions. The possible interval for the Higgs VEV that they found reproduces the EMPRESS ^4He abundance would, however, worsen the deviation for deuterium significantly.

Changing the Higgs VEV v influences all elementary particle masses as they scale linearly with v , assuming that the Yukawa couplings remain unchanged. This influences not only the neutron-proton mass difference, which is particularly significant for the ^4He abundance, but also the QCD scale Λ_{QCD} . Burns et al. take the latter into account [1]. While this is an important addition to the existing literature on the topic, we believe that the calculation can be improved in some parts, as shown here. In particular, the treatment of the neutron-proton mass difference, see Sect. II, and the quark mass dependence of the deuteron binding energy, see Sec. III, will be the subject of our work. The weak $n \leftrightarrow p$ rates are discussed in Sec. IV and the $n + p \rightarrow d + \gamma$ reaction is considered in Sec. V. Our results are displayed and discussed in Sec. VI. The Appendix contains some details on a one-boson-exchange model that can be used to study the deuteron for a varying Higgs VEV.

II. NEUTRON-PROTON MASS DIFFERENCE

The quark masses change linearly with the Higgs VEV and thus also the mass difference between up- and down-quark scales with $\delta v/v$. Throughout this work, we assume that the corresponding Yukawa couplings are constant. The neutron-proton mass difference has a QCD part coming from the quark mass difference and a QED part coming from Coulomb effects between the charged quarks in the nucleon. To a good approximation, the latter should stay constant under variation of the Higgs VEV. The QCD contribution to the $n - p$ mass difference is not, however, equal to just the quark mass difference¹ but has also contributions from the matrix element $\langle p | u\bar{u} - d\bar{d} | p \rangle$ [11]. This can be understood easily from the two-flavor QCD Hamiltonian, where the explicit chiral symmetry breaking originates from the mass term $m_u \bar{u}u + m_d \bar{d}d$, and the neutron-proton mass difference is given by its isovector component. In [12], the electromagnetic contribution to the neutron-proton mass difference was precisely determined using the Cottingham sum rule and the strong part can then be deduced from the physical mass splitting, leading to

$$m_{\text{QCD}} = 1.87 \mp 0.16 \text{ MeV} , \quad m_{\text{QED}} = -0.58 \pm 0.16 \text{ MeV} . \quad (1)$$

The neutron-proton mass difference as a function of the Higgs VEV should therefore be taken as

$$\frac{Q_N}{\text{MeV}} = \frac{m_n - m_p}{\text{MeV}} = (1.87 \mp 0.16) \left(1 + \frac{\delta v}{v} \right) - (0.58 \pm 0.16). \quad (2)$$

We note in passing that the separation of the strong from the electromagnetic contribution is afflicted with some problems, for a pedagogical discussion see [13].

III. PION MASS DEPENDENCE OF THE DEUTERON MASS AND THE NUCLEON-NUCLEON SCATTERING LENGTHS

Changing the quark masses influences of course also the pion mass. To first order in chiral perturbation theory the average pion mass can be found from the Gell-Mann-Oakes-Renner relation

$$M_\pi^2 = B_0(m_u + m_d) + \mathcal{O}((m_u \pm m_d)^2) , \quad (3)$$

where the quark masses scale linearly with $\delta v/v$ and the constant B_0 , which is related to the scalar singlet quark condensate, is taken to depend on δv like the QCD scale Λ_{QCD} , which [1] found to be proportional to $(1 + \delta v/v)^{0.25}$. The pion mass at a given value of the Higgs VEV is therefore

$$M_\pi = M_\pi^{\text{phys}} \left(1 + \frac{\delta v}{v} \right)^{1.25/2} . \quad (4)$$

¹ Note also that the light quark masses are not RG invariant and thus not observable.

Here, $M_\pi^{\text{phys}} = 138.03 \text{ MeV}$ is the physical average pion mass for the present value of v , that is $\delta v = 0$. For the Higgs VEV varying by $\pm 10\%$, that is $|\delta v/v| \leq 0.1$, the pion mass varies between 129 MeV and 147 MeV. A change in the pion mass affects also other physical quantities that are very relevant for BBN simulations – above all the average nucleon mass m_N . The axial vector coupling g_A as well as the pion decay constant (which will become relevant later) do also depend on M_π . One could use chiral perturbation theory for calculating the pion mass dependence of these parameters. However, for already moderate changes in the pion mass, chiral perturbation theory becomes inaccurate for certain observables. More precisely, most lattice data can be fit well with a linear function in M_π , see e.g. [14], and the pion mass dependence of g_A exhibits strong cancellations of one- and two-loop contributions [15]. We therefore fit a rational function to some lattice QCD data for these quantities at different values of M_π .

Consider first the nucleon mass m_N . We fit the data from Ref. [16] with a rational function

$$m_N(M_\pi^2) = m_N^{\text{phys}} + \frac{(3.63 \pm 0.19) \text{ GeV}^{-1} (M_\pi^2 - (M_\pi^{\text{phys}})^2)}{1 + (4.80 \pm 0.61) \text{ GeV}^{-2} (M_\pi^2 - (M_\pi^{\text{phys}})^2)}, \quad (5)$$

where $m_N^{\text{phys}} = 938.94 \text{ MeV}$ is the value of the physical nucleon mass, that is for $\delta v = 0$. We note, however, that in the range for the Higgs VEV variation discussed here, the third order chiral perturbation theory (ChPT) representation of m_N gives a pion mass variation consistent with the one from fitting to the lattice data. Still, we prefer to work with this fit function as it allows for larger variations in M_π and thus δv . Similarly, for the axial-vector coupling, the data from [17] are fitted with a polynomial

$$g_A(M_\pi^2) = g_A^{\text{phys}} - (2.19 \pm 0.27) \text{ GeV}^{-1} (M_\pi^2 - (M_\pi^{\text{phys}})^2) + (8.23 \pm 1.47) \text{ GeV}^{-3} (M_\pi^2 - (M_\pi^{\text{phys}})^2)^2. \quad (6)$$

Including only the more recent and more precise lattice QCD data from [18], one arrives instead at

$$g_A(M_\pi^2) = g_A^{\text{phys}} - (0.43 \pm 0.04) \text{ GeV}^{-1} (M_\pi^2 - (M_\pi^{\text{phys}})^2), \quad (7)$$

where $g_A^{\text{phys}} = 1.267$ denotes the physical value at $\delta v = 0$. In all these equations, M_π is given in GeV. The fit results for m_N (left panel) and g_A (right panel) are displayed together with the lattice data in Fig. 1. The bands correspond to 1σ -errors of the fit. Comparing both fits for the axial vector coupling, it is apparent that there is still quite some uncertainty when it comes to calculations on the lattice. We choose to work with the latter fit for g_A that includes the more recent data. Choosing one parametrization or the other has, however, very little effect on the following calculations, because the range of pion mass variations is much smaller than what is shown in the figure. Note also that the one-loop $\mathcal{O}(p^3)$ ChPT result strongly deviates from the fit already in the small range of pion mass variations considered here.

The axial-vector coupling enters as a parameter when computing the weak neutron-proton interaction rates (see below). A change in the average nucleon mass has, of course, wide-ranging effects in the BBN

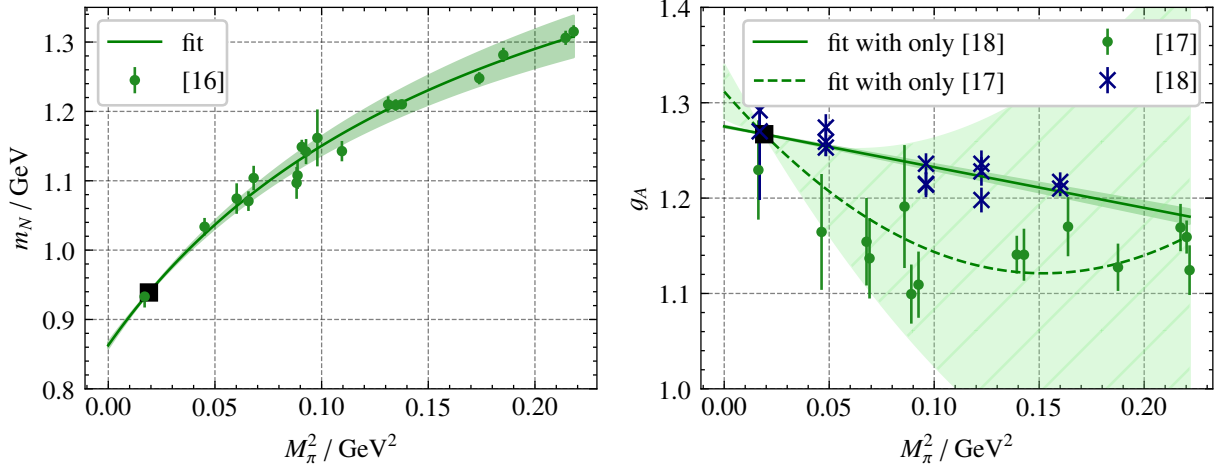


Figure 1: Rational function fit to lattice QCD data for the nucleon mass m_N ([16]) and the axial vector coupling g_A ([17, 18]) as a function of the pion mass squared. We forced the fits to go through the physical point (black filled square). The bands correspond to 1σ -errors of the fit. The dashed line and hatched band display the fit for g_A using only data from [17].

simulation. We change the neutron and proton mass so that they fulfill both the new value for the mass difference and the average mass:

$$m_p(\delta v) = m_N(\delta v) + Q_N(\delta v)/2, \quad (8)$$

$$m_n(\delta v) = m_p(\delta v) + Q_N(\delta v). \quad (9)$$

In [1] the deuteron binding energy was computed using a one-boson exchange model taken from [19]. The pion mass was scaled with the varying Higgs VEV as given above and the other meson masses as $(\delta v/v)^{0.25}$. It should be noted, however, that the quark mass dependence of the σ is more intricate than the one of a genuine quark-antiquark meson as worked out in detail in [20].

Here, we use lattice QCD results for the dependence of the deuteron binding energy on the pion mass. In Ref. [21], five data points for the nn and deuteron binding energy or scattering length were compiled and the so-called low-energy theorems (LETs), see e.g., [22, 23], were used to calculate the scattering length at a given pion mass from a binding energy obtained from lattice data without having information on the corresponding effective range. Note that at these pion masses, the nn system is also bound. Using this method and adding two recent lattice QCD data points from [24, 25], we get the pion mass dependence of the nucleon-nucleon scattering lengths in the S -wave channels and the deuteron binding energy by fitting a cubic polynomial to the obtained data. The corresponding results can be found in Figs. 2 and 3. The scattering lengths become relevant later for the $n + p \rightarrow d + \gamma$ reaction. In more detail, the deuteron binding

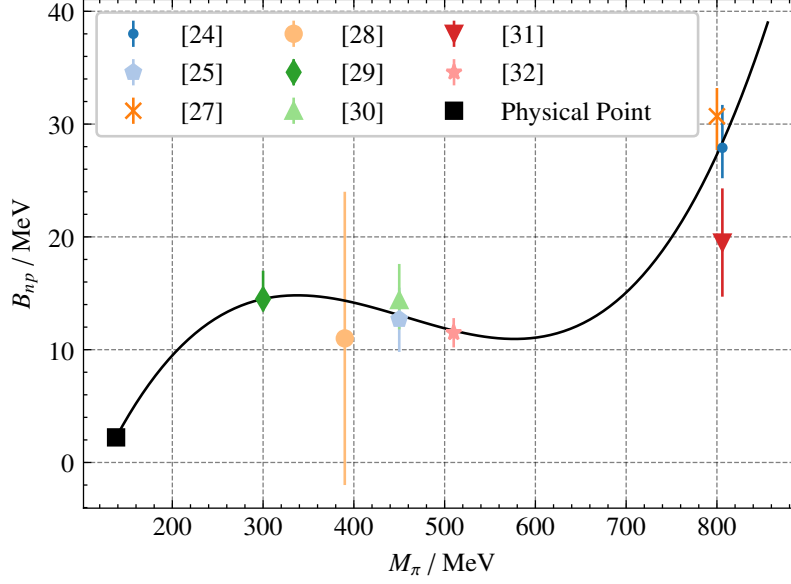


Figure 2: Cubic polynomial fit (black line) to lattice QCD data for the deuteron binding energy in the 3S_1 channel of nucleon-nucleon scattering. The fit was forced to go through the physical point.

energy as a function of $x = M_\pi - M_\pi^{\text{phys}}$ is given by

$$B_d(M_\pi) = B_d(M_\pi^{\text{phys}}) + 0.149x - 5.414 \times 10^{-4} \text{ MeV}^{-1} x^2 + 5.651 \times 10^{-7} \text{ MeV}^{-2} x^3, \quad (10)$$

where all masses are given in units of MeV. We note that the situation about the deuteron being bound is still a disputed issue in lattice QCD, see e.g [26], thus we forced the fit to go to the physical value for the physical pion mass. Further, the inverse scattering length in the 1S_0 channel is

$$a_s^{-1}(M_\pi) = a_s^{-1}(M_\pi^{\text{phys}}) + 3.762 \times 10^{-3} \text{ MeV}^{-1} x - 1.055 \times 10^{-5} \text{ MeV}^{-2} x^2 + 8.958 \times 10^{-9} \text{ MeV}^{-3} x^3, \quad (11)$$

while the inverse scattering length in the 3S_1 channel (corresponding to the deuteron) is given by

$$a_t^{-1}(M_\pi) = a_t^{-1}(M_\pi^{\text{phys}}) + 2.129 \times 10^{-3} \text{ MeV}^{-1} \text{ fm}^{-1} x - 6.789 \times 10^{-6} \text{ MeV}^{-2} \text{ fm}^{-1} x^2 + 6.672 \times 10^{-9} \text{ MeV}^{-3} \text{ fm}^{-1} x^3. \quad (12)$$

Calculating the deuteron binding energy in this way for different values of the Higgs VEV yields a similar result to what was found in [1] as can be seen from comparing Fig. 4 to Fig. 2 of [1]. It is unclear to us why these results are so similar. Using a more sophisticated one-boson-exchange model, we indeed find a different result as discussed in the Appendix.

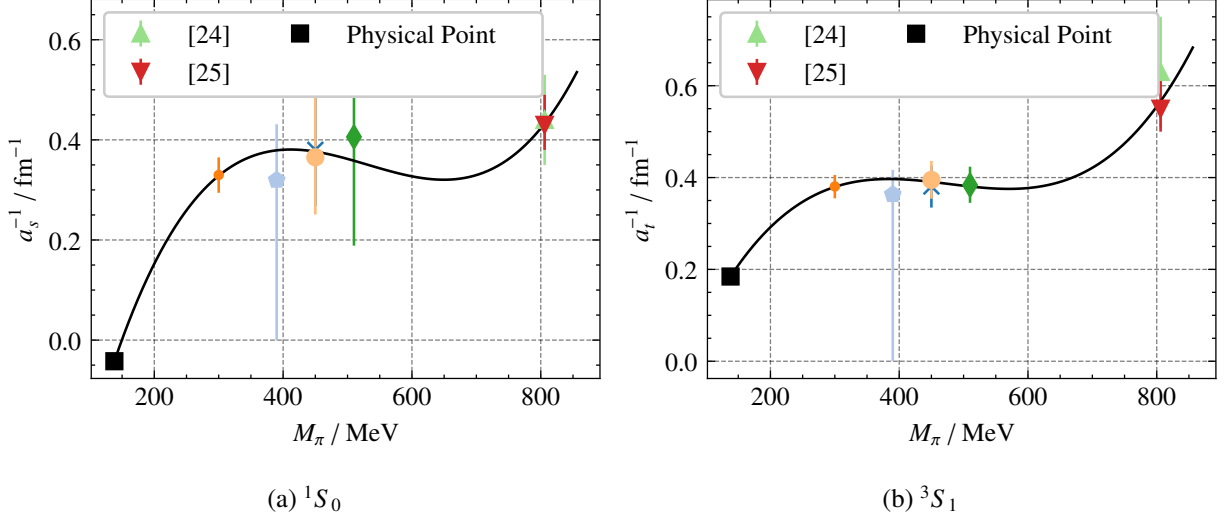


Figure 3: Cubic polynomial fit (black line) to inverse scattering length resulting from the LET calculations in the 1S_0 and the 3S_1 channel of nucleon-nucleon scattering. The data points from Refs. [24] and [25] are direct lattice QCD results. The fit was forced to go through the physical point.

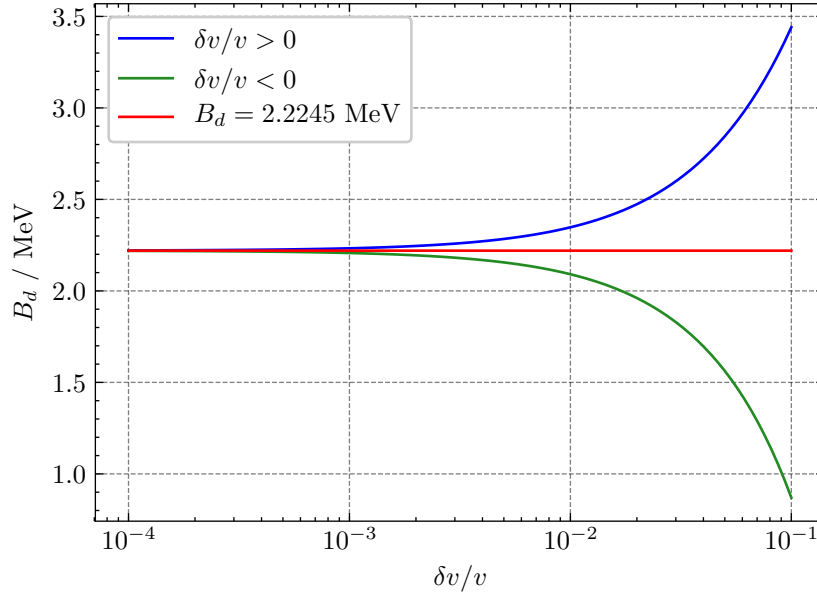


Figure 4: Deuteron binding energy as a function of the Higgs VEV, calculated using Eqs. (4,10).

IV. WEAK $n \leftrightarrow p$ RATES

Before the universe is cool enough for deuterium fusion to be efficient and for BBN to actually start, the weak interactions between neutrons and protons are dominant. Because especially the ^4He abundance is very sensitive to the number of neutrons existing at the beginning of BBN, it is quite important to accurately

calculate the neutron-proton interaction rates. In [1] effects from a changing electron mass are included (as noted before, m_e also scales linearly with δv) on the thermal background as well as the change in the W -boson mass that modifies the Fermi constant G_F :

$$G_F = \frac{\sqrt{2}}{8} \frac{g^2}{M_W^2} = \frac{1}{\sqrt{2}v^2} \rightarrow G_F(\delta v) = G_F(0) \left(1 + \frac{\delta v}{v}\right)^{-2}. \quad (13)$$

The relevant Higgs VEV dependent part of the neutron lifetime is given by

$$\tau_n \sim \frac{1}{\mathcal{G}f_R}, \quad \mathcal{G} = \frac{(G_F V_{ud})^2 (1 + 3g_A^2)}{2\pi^3} m_e^5, \quad (14)$$

where f_R is the integral over the Fermi energy spectrum. For small temperatures one can ignore temperature-dependent effects from the neutrino and electron Fermi distribution functions when calculating the neutron β -decay rate. So, in this approximation, f_R is given by [33]

$$f_R = \frac{1}{m_e^5} \int_0^{p_{e,\max}} \left(Q_n - \sqrt{m_e^2 + p_e^2}\right)^2 F(Z, p_e) p_e^2 dp_e, \quad (15)$$

$$= \int_0^{x_{\max}} \left(\sqrt{1+x_0^2} - \sqrt{1+x^2}\right)^2 x^2 dx, \text{ where } x = \frac{p_e}{m_e} \text{ and } x_0 = \sqrt{\left(\frac{Q_n}{m_e}\right)^2 - 1}. \quad (16)$$

$F(Z, p_e)$ is the Fermi function including Coulomb effects between the charged electron or positron and the proton in the final state. Of course, one could also include QED radiative corrections, finite-mass, electroweak magnetism and finite-temperature effects, all of which were considered in the calculation of the weak $n \leftrightarrow p$ rates in PRyMordial [8]. Because these are higher order effects, we will not include them in the Higgs VEV correction to the neutron lifetime. At high temperatures the Fermi functions of the neutrino and the electron cannot be ignored, thus one has to recompute the weak neutron-proton rates every time one changes the relevant parameters (see also [34] for a detailed discussion).

We assume that in [1] the authors did not account for the change in the neutron lifetime that comes from the Fermi integral as they do not mention changing the neutron lifetime at all but merely including the changes in the Fermi constant G_F and in the electron mass m_e . But because the neutron-proton mass difference as well as the electron mass changes with δv , the variation in f_R influences the neutron lifetime significantly. As mentioned above, the axial-vector coupling depends on the pion mass and therefore also on the Higgs VEV which should be included in the calculation.

We therefore recalculate the $n \leftrightarrow p$ weak rates for every value of $\delta v/v$ changing the electron, neutron and proton mass as mentioned above as well as G_F and g_A . The neutron lifetime changes according to

$$\tau_n(\delta v) = \tau_n(0) \frac{\mathcal{G}(0)f_R(0)}{\mathcal{G}(\delta v)f_R(\delta v)}. \quad (17)$$

In Fig. 5 the fractional change in the $n \leftrightarrow p$ rates obtained from our calculation is displayed. Fig. 6 shows the neutron lifetime as a function of the Higgs VEV. We observe a significant variation from the experimental

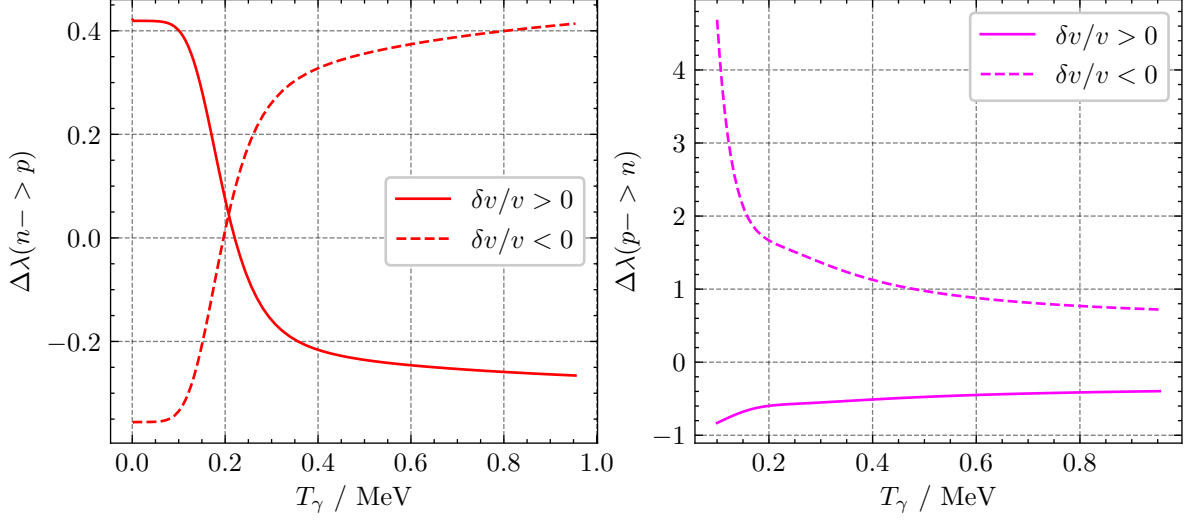


Figure 5: Fractional change in the weak $n \leftrightarrow p$ reaction rates including all relevant effects.

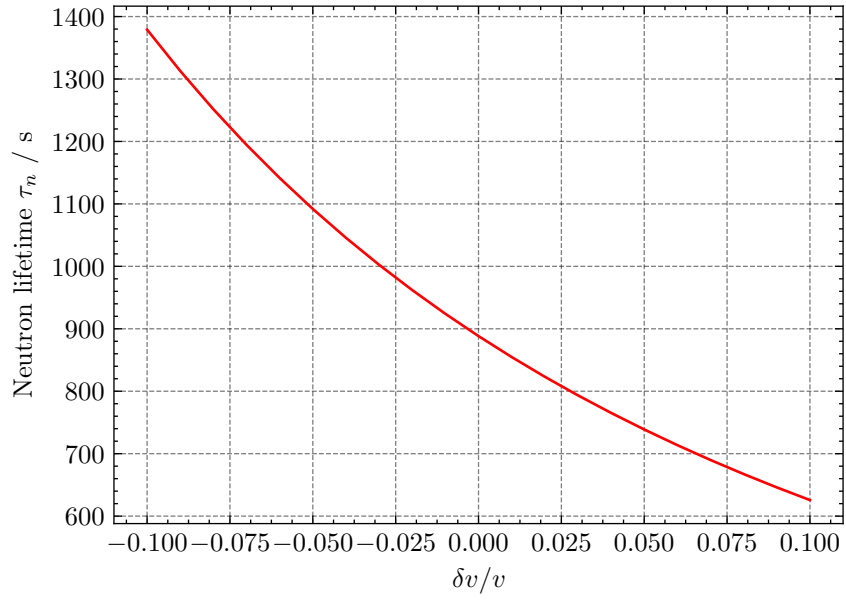


Figure 6: The neutron lifetime τ_n as a function of the Higgs VEV variation $\delta v/v$.

value at $\delta v = 0$, which is $\tau_n = 878.4$ s [10]. The linear behaviour for the fractional change in the rates that was observed in [1] we do not see, and we can also not reproduce it given the description of their calculation.

V. THE $n + p \rightarrow d + \gamma$ REACTION

Finally, we can use the pionless effective field theory (EFT) approach by [35] for calculating the $n + p \rightarrow d + \gamma$ reaction rate, which is the first nuclear reaction taking place in BBN and therefore quite important. In

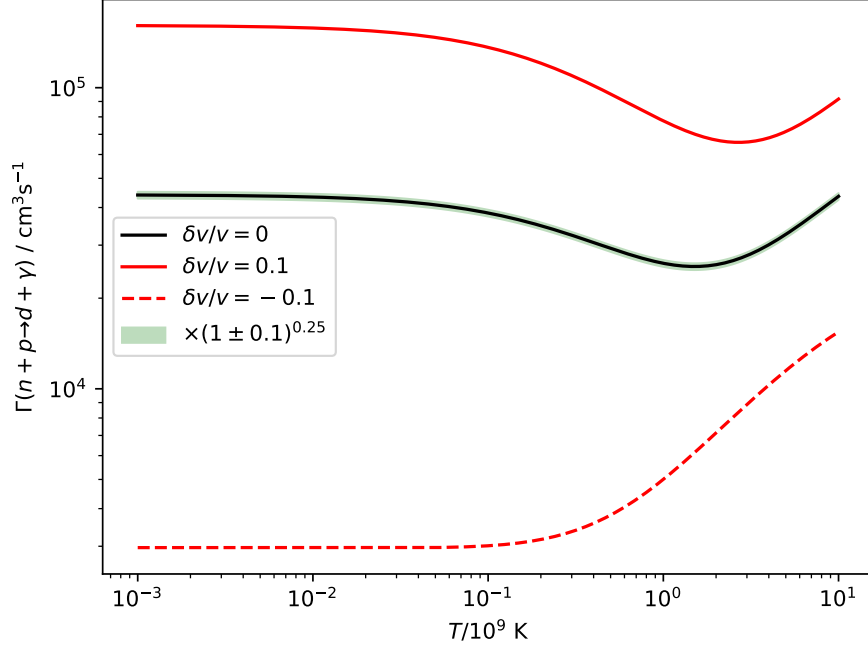


Figure 7: Reaction rate for $n + p \rightarrow d + \gamma$ for $\delta v/v = 0, \pm 0.1$ calculated from pionless EFT [35] with nuclear parameters changed as described in the text. The shaded green band gives the original rate multiplied by $(1 \pm 0.1)^{0.25}$, so the range in which the $n + p \rightarrow d + \gamma$ rate varies in the calculation of [1].

[1], it is assumed that all nuclear reaction rates scale like Λ_{QCD} , so a factor of $(1 + \delta v/v)^{0.25}$ is multiplied to every rate. While this might be a reasonable approximation, one can make use of the analytic expression for the $n + p \rightarrow d + \gamma$ rate from [35] and plug in the nucleon mass, the 1S_0 scattering length, the deuteron binding energy and the effective range ρ_d at a given value of the Higgs VEV. The deuteron effective range can be found from the binding energy and the triplet scattering length a_t via:

$$\rho_d = 2 \frac{a_t \sqrt{B_d m_N} - 1}{a_t m_N B_d} . \quad (18)$$

The effective range of the 1S_0 channel only comes in at higher orders and we can safely ignore changes in this parameter as well as possible scale effects in the isoscalar contributions to the cross section. The resulting reaction rate for $\delta v/v = 0, \pm 0.1$ is shown in Fig. 7. Changing the Higgs VEV therefore has a huge impact on the $n + p \rightarrow d + \gamma$ reaction. We also see that the functional form is not consistent with a simple scaling with $(1 + \delta v/v)^{0.25}$.

Before presenting our final results, let us summarize the differences in our calculation to the one in [1]. First, we use an updated form of the neutron-proton mass difference, as given by Eq. (2). Second, the quark mass dependence of the deuteron binding energy is obtained from lattice QCD data with the help of the

	${}^4\text{He}$	d
PDG	$\delta v/v \in [-0.0006, 0.0417]$	$\delta v/v \in [-0.0045, -0.0011]$
EMPRESS	$\delta v/v \in [0.0257, 0.0711]$	
PDG	$\delta v/v \in [-0.0006, 0.0393]$	$\delta v/v \in [-0.0593, -0.0123]$
EMPRESS	$\delta v/v \in [0.0239, 0.0684]$	

Table I: Upper panel: Constraints on the Higgs VEV variation $\delta v/v$ derived from 2σ bounds of the observed values given in the PDG [10] and by the EMPRESS collaboration [9] for the abundances of ${}^4\text{He}$ and deuterium. Lower panel: Constraints obtained from a calculation where $n + p \rightarrow d + \gamma$ is treated like in [1], see Fig. 9.

nucleon-nucleon scattering LETs [22, 23], whereas in [1] a one-boson exchange model was used with the appropriate scalings of the various meson exchanges. Interestingly, the resulting Higgs VEV dependence of the deuteron binding energy comes out very similar in both approaches. We also used lattice QCD data to model the pion-mass-dependence of the nucleon mass and the axial vector current, which was not taken into account in [1]. Then, we included the change in the Fermi-integral appearing in the neutron lifetime, see Eqs. (14) and (15) which altered the Higgs VEV dependence of the light element abundances significantly. Finally, we made use of the pionless EFT approach by [35] to include effects of a varying Higgs VEV on the $n + p \rightarrow d + \gamma$ rate, as explained in this section.

VI. RESULTS

Finally, putting everything together, our results can be found in Fig. 8. What is most noticeable is the behaviour of the deuterium abundance: it increases drastically for negative values of $\delta v/v$. Also, both the ${}^4\text{He}$ and deuterium abundance behave in exactly the opposite way as was calculated in [1]: they increase for negative $\delta v/v$. This is due to the change in the neutron lifetime that was ignored in [1]. The improved constraints for the Higgs VEV variation that can be derived by our calculation are collected in Tab. I.

In Fig. 9 we show the evolution of the abundances for different values of the Higgs VEV not including effects from the $n + p \rightarrow d + \gamma$ rate as would be implied by [35] but scaling it like all other rates proportional to the QCD scale Λ_{QCD} , i.e as $\sim (1 + \delta v/v)^{0.25}$. The result for the deuterium abundance is markedly different from the more realistic calculation.

Nonetheless, we can confirm the result of [1] that tuning the Higgs VEV so that the predicted ${}^4\text{He}$ abundance matches the new EMPRESS result would worsen the deviation between theory and experiment for the deuterium abundance significantly.

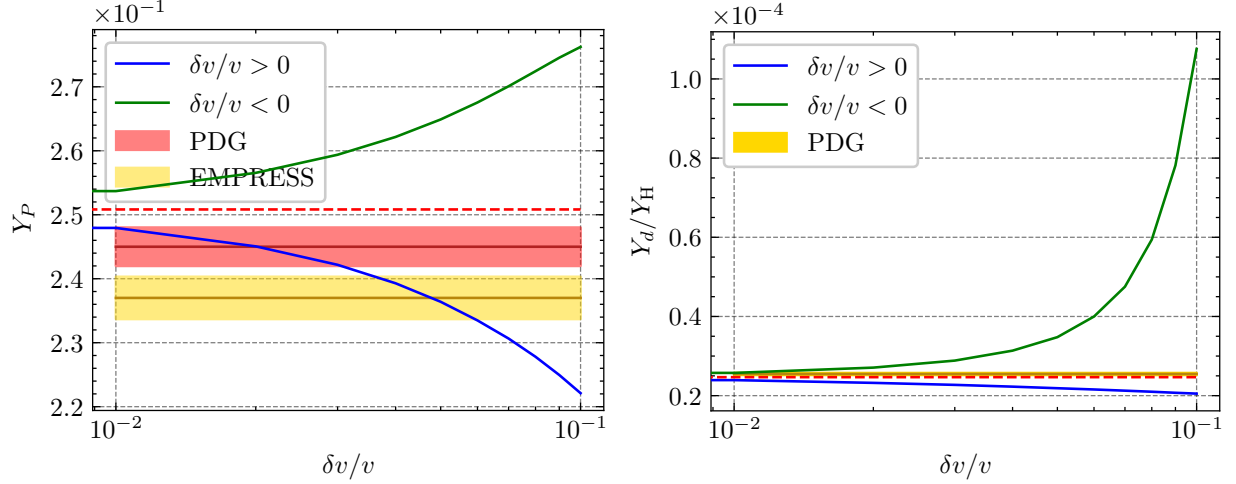


Figure 8: ${}^4\text{He}$ (left) and d (right) abundance as a function of $\delta v/v$.

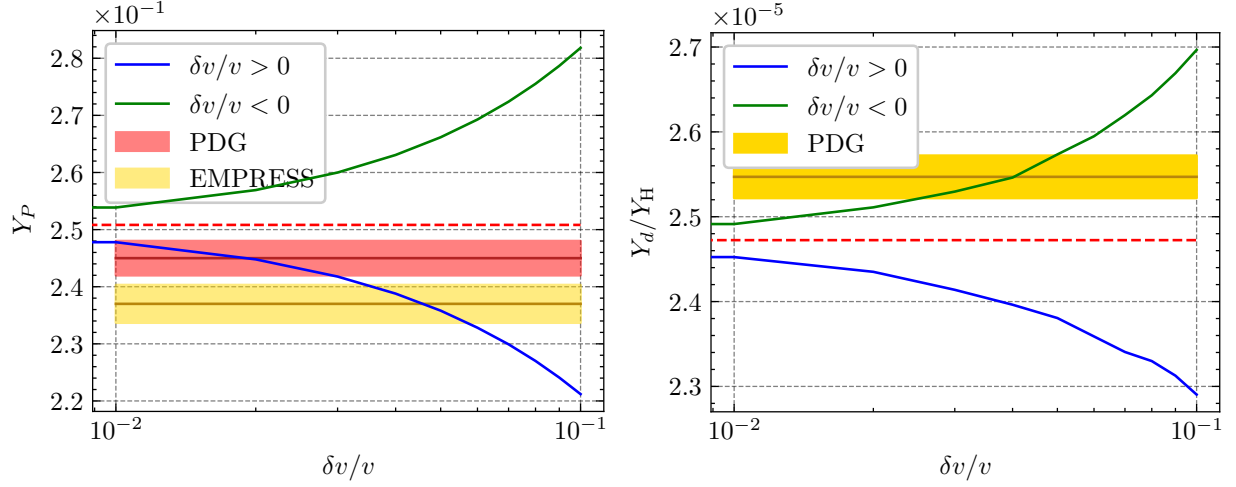


Figure 9: ${}^4\text{He}$ (left) and d (right) abundance as a function of $\delta v/v$ not including changes in the $n + p \rightarrow d + \gamma$ rate as would be implied by pionless EFT but scaling it like Λ_{QCD} .

ACKNOWLEDGEMENTS

We would like to thank Bernard Metsch for helpful discussions. This work was supported in part by the European Research Council (ERC) under the European Union's Horizon 2020 research and innovation programme (grant agreement No. 101018170), by DFG and NSFC through funds provided to the Sino-German CRC 110 "Symmetries and the Emergence of Structure in QCD" (NSFC Grant No. 11621131001, DFG Grant No. TRR110). The work of UGM was supported in part by the CAS President's International Fellowship Initiative (PIFI) (Grant No. 2018DM0034).

Appendix A: Deuteron binding energy from a one-boson-exchange potential

In Sect. III we used lattice QCD data to model the pion-mass dependence of the deuteron binding energy which was similar to the dependence found in [1] from calculating the binding energy using a one-boson exchange potential (OBEP). Unfortunately, the authors of [1] do not describe the particular form of the potential they used in detail. We try to confirm their results by implementing the OBEP potential described in [36], where also contributions from ρ -meson exchange are considered. For more details, we refer to the textbook [37] (and references therein). In [36], the small contribution from the D -wave for the 3S_1 -channel is neglected, that is one works strictly with angular momentum $L = 0$. The potentials corresponding to the different meson exchanges are then given in coordinate space as:

$$V_\pi(r) = (\tau_1 \cdot \tau_2)(\sigma_1 \cdot \sigma_2) \frac{g_{\pi NN}^2}{4\pi} \frac{1}{12} \left(\frac{M_\pi}{m_N} \right)^2 \frac{e^{-M_\pi r}}{r}, \quad (\text{A1})$$

$$V_\sigma(r) = -\frac{g_{\sigma NN}^2}{4\pi} \left(1 - \frac{1}{4} \left(\frac{M_\sigma}{m_N} \right)^2 \right) \frac{e^{-M_\sigma r}}{r}, \quad (\text{A2})$$

$$V_\omega(r) = \frac{g_{\omega NN}^2}{4\pi} \left(1 + \frac{1}{2} \left(\frac{M_\omega}{m_N} \right)^2 \left[1 + \frac{1}{3} (\sigma_1 \cdot \sigma_2) \right] \right) \frac{e^{-M_\omega r}}{r}, \quad (\text{A3})$$

$$V_\rho(r) = (\tau_1 \cdot \tau_2) \frac{g_{\rho NN}^2}{4\pi} \left(1 + \frac{1}{2} \left(\frac{M_\rho}{m_N} \right)^2 \left[1 + \frac{g_T^\rho}{g_{\rho NN}} + \frac{1}{3} \left(1 + \frac{g_T^\rho}{g_{\rho NN}} \right)^2 (\sigma_1 \cdot \sigma_2) \right] \right) \frac{e^{-M_\rho r}}{r}. \quad (\text{A4})$$

Here, m_N is the average nucleon mass. The potential depends on the total spin S and total isospin I of the channel through the factors $(\sigma_1 \cdot \sigma_2) = 2S(S+1) - 3$ and $(\tau_1 \cdot \tau_2) = 2I(I+1) - 3$. The full potential is then

$$V_{\text{OBE}}(r) = \sum_{\alpha=\{\pi,\sigma,\omega,\rho\}} V_\alpha(r) + \frac{1}{4\pi} \frac{e^{-\Lambda r}}{r}, \quad (\text{A5})$$

where the cutoff Λ regularizes the UV-divergence. In general, one takes different cut-offs for different mesons, but since we are only interested in the deuteron binding energy, this simplified form suffices. The physical values for the meson mass are

$$M_\pi = 139.57 \text{ MeV}, \quad M_\sigma = 550 \text{ MeV}, \quad M_\omega = 783 \text{ MeV}, \quad M_\rho = 769 \text{ MeV}, \quad (\text{A6})$$

and they are scaled with the Higgs VEV as explained in [1]: the pion mass with $(\delta v/v)^{1.25/2}$ and the other masses as $(\delta v/v)^{0.25}$. The coupling constant $g_{\pi NN}$ is taken from the Goldberger-Treiman discrepancy [38]

$$g_{\pi NN}(\delta v) = \frac{g_A(\delta v)m_N(\delta v)}{F_\pi(\delta v)} \left(1 - \frac{2M_\pi^2(\delta v)\bar{d}_{18}}{g_A(\delta v)} \right), \quad \bar{d}_{18} = -0.47 \text{ GeV}^{-2}, \quad (\text{A7})$$

where m_N are g_A given in Eqs. (5) and (7) as a function of the pion mass. $F_\pi(M_\pi)$ can also be found from a fit to lattice data by [39]:

$$F_\pi(M_\pi) = F_\pi^{\text{phys}} + (0.138 \pm 0.009) \text{ GeV}^{-1} (M_\pi^2 - (M_\pi^{\text{phys}})^2) - (0.068 \pm 0.043) \text{ GeV}^{-3} (M_\pi^2 - (M_\pi^{\text{phys}})^2)^2, \quad (\text{A8})$$

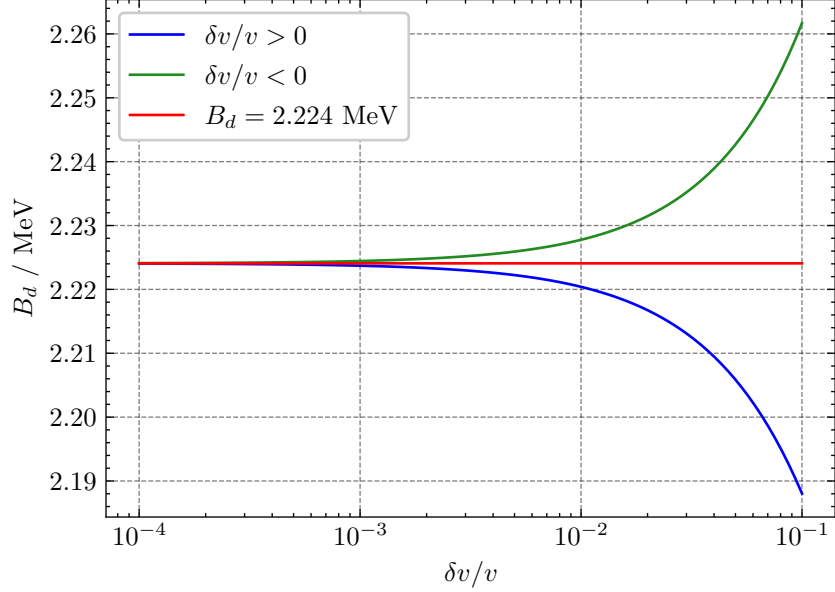


Figure 10: Deuteron binding energy as a function of $\delta v/v$ calculated using the OBEP from [36].

with M_π given in GeV. Finally, we use the coupling constants given in [36] as parameter set I:

$$\frac{g_{\sigma NN}^2}{4\pi} = 14.17, \quad \frac{g_{\omega NN}^2}{4\pi} = 20.0, \quad \frac{g_{\rho NN}^2}{4\pi} = 0.80, \quad \Lambda = 1364 \text{ MeV} \quad (\text{A9})$$

and $g_T^\rho/g_{\rho NN} = 6.1$, and the tiny ω tensor coupling is neglected. The resulting change in the deuteron binding energy, when we vary the Higgs VEV by $\pm 10\%$, is much smaller than what was given in [1] and also has the opposite sign, see Fig. 10. Note further that keeping $g_{\pi NN}$ constant instead of varying it as in Eq.(A7) has only a mild influence on the results.

Plugging in this deuteron binding energy dependence, we find that the $n + p \rightarrow d + \gamma$ rate does not vary as much as before and resembles more the $(1 + \delta v/v)^{0.25}$ -scaling that was used in [1]. This is presented in Fig. 11.

The resulting ^4He and d abundances for this calculation can be found in Fig. 12. They are close to the results obtained by simply scaling the $n + p \rightarrow d + \gamma$ rate as described in [1], which is evident when comparing Fig. 12 to Fig. 9.

-
- [1] A.-K. Burns, V. Keus, M. Sher, and T. M. P. Tait, Constraints on variation of the weak scale from big bang nucleosynthesis (2024), arXiv:2402.08626 [hep-ph].
 - [2] C. J. Hogan, Why the universe is just so, *Reviews of Modern Physics* **72**, 1149–1161 (2000).
 - [3] J.-P. Uzan, The fundamental constants and their variation: observational and theoretical status, *Reviews of Modern Physics* **75**, 403–455 (2003).

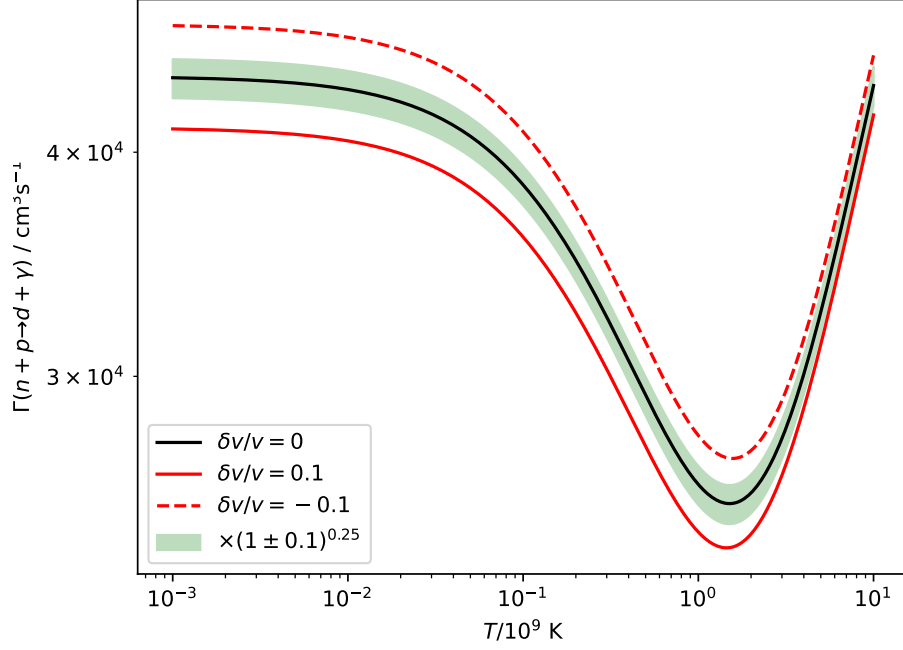


Figure 11: Reaction rate for $n + p \rightarrow d + \gamma$ for $\delta v/v = 0, \pm 0.1$ calculated from pionless effective field theory [35] with nuclear parameters changed as described in the text, but the binding energy taken from a OBEP calculation. The shaded green band gives the original rate multiplied by $(1 \pm 0.1)^{0.25}$, so the range in which the $n + p \rightarrow d + \gamma$ rate varies in the calculation of [1].

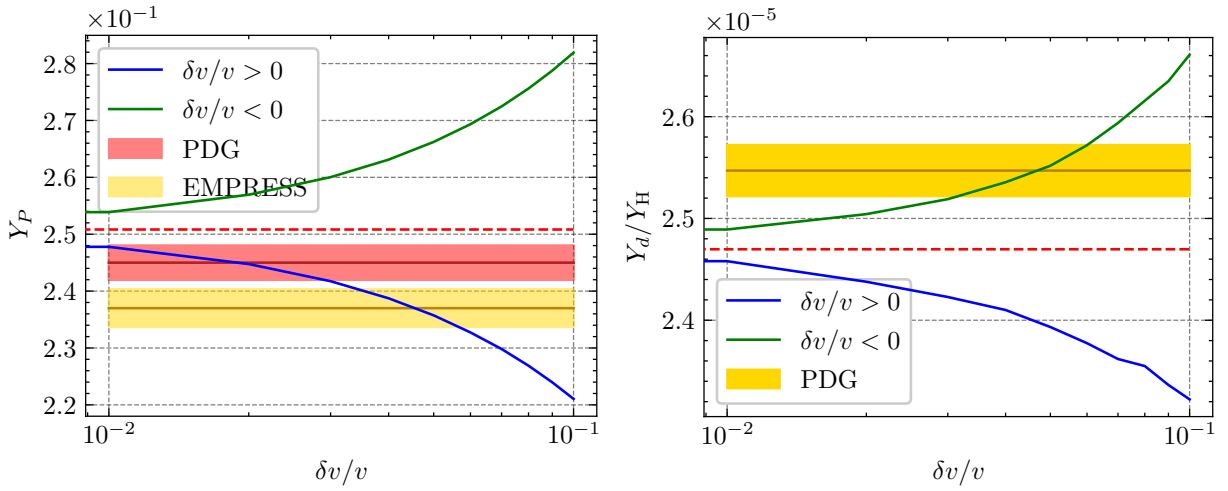


Figure 12: ${}^4\text{He}$ (left) and deuterium (right) abundance as a function of $\delta v/v$ for the deuteron binding energy calculated using an OBEP.

- [4] A. N. Schellekens, Life at the interface of particle physics and string theory, *Reviews of Modern Physics* **85**, 1491–1540 (2013).
- [5] U.-G. Meißner, Anthropic considerations in nuclear physics, *Science Bulletin* **60**, 43–54 (2015).
- [6] J. F. Donoghue, The multiverse and particle physics, *Annual Review of Nuclear and Particle Science* **66**, 1–21 (2016).
- [7] F. C. Adams, The degree of fine-tuning in our universe — and others, *Physics Reports* **807**, 1–111 (2019).
- [8] A.-K. Burns, T. M. P. Tait, and M. Valli, Prymordial: The first three minutes, within and beyond the standard model (2023), arXiv:2307.07061 [hep-ph].
- [9] A. Matsumoto, M. Ouchi, K. Nakajima, M. Kawasaki, K. Murai, K. Motohara, Y. Harikane, Y. Ono, K. Kushibiki, S. Koyama, S. Aoyama, M. Konishi, H. Takahashi, Y. Isobe, H. Umeda, Y. Sugahara, M. Onodera, K. Nagamine, H. Kusakabe, Y. Hirai, T. J. Moriya, T. Shibuya, Y. Komiyama, K. Fukushima, S. Fujimoto, T. Hattori, K. Hayashi, A. K. Inoue, S. Kikuchihiro, T. Kojima, Y. Koyama, C.-H. Lee, K. Mawatari, T. Miyata, T. Nagao, S. Ozaki, M. Rauch, T. Saito, A. Suzuki, T. T. Takeuchi, M. Umemura, Y. Xu, K. Yabe, Y. Zhang, and Y. Yoshii, Empress. viii. a new determination of primordial he abundance with extremely metal-poor galaxies: A suggestion of the lepton asymmetry and implications for the hubble tension, *The Astrophysical Journal* **941**, 167 (2022).
- [10] R. L. Workman *et al.*, Review of Particle Physics, *PTEP* 10.1093/ptep/ptac097 (2022), 083C01, <https://academic.oup.com/ptep/article-pdf/2022/8/083C01/49175539/ptac097.pdf>.
- [11] J. Gasser and H. Leutwyler, Quark Masses, *Phys. Rept.* **87**, 77 (1982).
- [12] J. Gasser, H. Leutwyler, and A. Rusetsky, On the mass difference between proton and neutron, *Phys. Lett. B* **814**, 136087 (2021), arXiv:2003.13612 [hep-ph].
- [13] U.-G. Meißner and A. Rusetsky, *Effective Field Theories* (Cambridge University Press, 2022).
- [14] A. Walker-Loud, Nuclear Physics Review, *PoS LATTICE2013*, 013 (2014), arXiv:1401.8259 [hep-lat].
- [15] V. Bernard and U.-G. Meißner, The Nucleon axial-vector coupling beyond one loop, *Phys. Lett. B* **639**, 278 (2006), arXiv:hep-lat/0605010.
- [16] C. Alexandrou, M. Constantinou, V. Drach, K. Jansen, C. Kallidonis, and G. Koutsou, Nucleon generalized form factors with twisted mass fermions, *PoS LATTICE2013*, 292 (2014), arXiv:1312.2874 [hep-lat].
- [17] C. Alexandrou, M. Constantinou, K. Hadjiyiannakou, K. Jansen, C. Kallidonis, and G. Koutsou, Nucleon observables and axial charges of other baryons using twisted mass fermions, *PoS LATTICE2014*, 151 (2015), arXiv:1411.3494 [hep-lat].
- [18] C. C. Chang *et al.*, A per-cent-level determination of the nucleon axial coupling from quantum chromodynamics, *Nature* **558**, 91 (2018), arXiv:1805.12130 [hep-lat].
- [19] U.-G. Meißner, Low-energy hadron physics from effective chiral lagrangians with vector mesons, *Physics Reports* **161**, 213 (1988).
- [20] C. Hanhart, J. R. Pelaez, and G. Rios, Quark mass dependence of the rho and sigma from dispersion relations and Chiral Perturbation Theory, *Phys. Rev. Lett.* **100**, 152001 (2008), arXiv:0801.2871 [hep-ph].
- [21] T. A. Lähde, U.-G. Meißner, and E. Epelbaum, An update on fine-tunings in the triple-alpha process, *Eur. Phys.*

- J. A **56**, 89 (2020), arXiv:1906.00607 [nucl-th].
- [22] V. Baru, E. Epelbaum, A. A. Filin, and J. Gegelia, Low-energy theorems for nucleon-nucleon scattering at unphysical pion masses, Phys. Rev. C **92**, 014001 (2015), arXiv:1504.07852 [nucl-th].
 - [23] V. Baru, E. Epelbaum, and A. A. Filin, Low-energy theorems for nucleon-nucleon scattering at $M_\pi = 450$ MeV, Phys. Rev. C **94**, 014001 (2016), arXiv:1604.02551 [nucl-th].
 - [24] M. L. Wagman, F. Winter, E. Chang, Z. Davoudi, W. Detmold, K. Orginos, M. J. Savage, and P. E. Shanahan, Baryon-Baryon Interactions and Spin-Flavor Symmetry from Lattice Quantum Chromodynamics, Phys. Rev. D **96**, 114510 (2017), arXiv:1706.06550 [hep-lat].
 - [25] M. Illa *et al.* (NPLQCD), Low-energy scattering and effective interactions of two baryons at $m_\pi \sim 450$ MeV from lattice quantum chromodynamics, Phys. Rev. D **103**, 054508 (2021), arXiv:2009.12357 [hep-lat].
 - [26] S. Amarasinghe, R. Baghdadi, Z. Davoudi, W. Detmold, M. Illa, A. Parreno, A. V. Pochinsky, P. E. Shanahan, and M. L. Wagman, Variational study of two-nucleon systems with lattice QCD, Phys. Rev. D **107**, 094508 (2023), arXiv:2108.10835 [hep-lat].
 - [27] E. Berkowitz, T. Kurth, A. Nicholson, B. Joo, E. Rinaldi, M. Strother, P. M. Vranas, and A. Walker-Loud, Two-Nucleon Higher Partial-Wave Scattering from Lattice QCD, Phys. Lett. B **765**, 285 (2017), arXiv:1508.00886 [hep-lat].
 - [28] S. R. Beane, E. Chang, W. Detmold, H. W. Lin, T. C. Luu, K. Orginos, A. Parreno, M. J. Savage, A. Torok, and A. Walker-Loud (NPLQCD), The Deuteron and Exotic Two-Body Bound States from Lattice QCD, Phys. Rev. D **85**, 054511 (2012), arXiv:1109.2889 [hep-lat].
 - [29] T. Yamazaki, K.-i. Ishikawa, Y. Kuramashi, and A. Ukawa, Study of quark mass dependence of binding energy for light nuclei in 2+1 flavor lattice QCD, Phys. Rev. D **92**, 014501 (2015), arXiv:1502.04182 [hep-lat].
 - [30] K. Orginos, A. Parreno, M. J. Savage, S. R. Beane, E. Chang, and W. Detmold, Two nucleon systems at $m_\pi \sim 450$ MeV from lattice QCD, Phys. Rev. D **92**, 114512 (2015), [Erratum: Phys.Rev.D 102, 039903 (2020)], arXiv:1508.07583 [hep-lat].
 - [31] S. R. Beane *et al.* (NPLQCD), Nucleon-Nucleon Scattering Parameters in the Limit of SU(3) Flavor Symmetry, Phys. Rev. C **88**, 024003 (2013), arXiv:1301.5790 [hep-lat].
 - [32] T. Yamazaki, K.-i. Ishikawa, Y. Kuramashi, and A. Ukawa, Helium nuclei, deuteron and dineutron in 2+1 flavor lattice QCD, Phys. Rev. D **86**, 074514 (2012), arXiv:1207.4277 [hep-lat].
 - [33] E. Segrè, *Nuclei and Particles*, Vol. 2 (Basic Books, 1964) p. 507.
 - [34] U.-G. Meißner, B. C. Metsch, and H. Meyer, The electromagnetic fine-structure constant in primordial nucleosynthesis revisited, Eur. Phys. J. A **59**, 223 (2023), arXiv:2305.15849 [hep-th].
 - [35] G. Rupak, Precision calculation of $np \rightarrow d\gamma$ cross section for big-bang nucleosynthesis, Nucl. Phys. A **678**, 405 (2000).
 - [36] D. Lee, U.-G. Meißner, K. A. Olive, M. Shifman, and T. Vonk, θ -dependence of light nuclei and nucleosynthesis, Phys. Rev. Res. **2**, 033392 (2020), arXiv:2006.12321 [hep-ph].
 - [37] T. E. O. Ericson and W. Weise, *Pions and Nuclei* (Clarendon Press, Oxford, UK, 1988).
 - [38] N. Fettes, U.-G. Meißner, and S. Steininger, Pion - nucleon scattering in chiral perturbation theory. 1. Isospin

- symmetric case, Nucl. Phys. A **640**, 199 (1998), arXiv:hep-ph/9803266.
- [39] S. Dürr, Z. Fodor, C. Hoelbling, S. Krieg, T. Kurth, L. Lellouch, T. Lippert, R. Malak, T. Métivet, A. Portelli, A. Sastre, and K. Szabó (Budapest-Marseille-Wuppertal Collaboration), Lattice qcd at the physical point meets $su(2)$ chiral perturbation theory, Phys. Rev. D **90**, 114504 (2014).